This article has been accepted for publication in a future issue of this journal, but has not been fully edited. Content may change prior to final publication. Citation information: DOI 10.1109/TCOMM.2018.2817222, IEEE Transactions on Communications

Coordinated Beamforming for Downlink Visible Light Communication Networks

Hao Ma[1], Ayman Mostafa[1], Lutz Lampe[1] and Steve Hranilovic[2]
[1] Department of Electrical and Computer Engineering, University of British Columbia, Vancouver, Canada
[2] Department of Electrical and Computer Engineering, McMaster University

***Abstract*—Visible light communication (VLC) is an emerging short-range optical wireless communication technology that is driven by the widespread deployment of light-emitting diodes (LEDs). Indoor VLC users may experience noticeable interference when independent transmitters utilizing wide-beam luminaires are closely located. In this paper, a coordinated beamforming (CB) scheme is proposed for downlink interference mitigation among coexisting VLC attocells utilizing multi-luminaire transmitters. Compared to joint transmission (JT) schemes, wherein the data and channel state information are shared among transmitters of different attocells, the proposed CB scheme places lower requirements on the network in terms of backbone traffic, and is easier to implement in a practical deployment, though at the cost of compromised performance. In this paper, we investigate the downlink transmission of coordinated VLC attocells and focus on its transmitter design. The weighted sum mean square error (WSMSE) is adopted as the performance metric to take into consideration interference, noise, and fairness among users in system optimization. The WSMSE minimization problem is considered with linear beamforming restricted by amplitude constraints. Such constraints arise from dynamic range limitations in typical LEDs. Moreover, we extend our design method to take into account possible mismatches in channel information available to the transmitters. Numerical examples are provided to illustrate the performance of the proposed CB scheme in typical VLC scenarios. We also quantify the performance gap among several coordination schemes including JT and CB.**

***Index Terms*—Visible light communication, Precoding, Cooperative communication**

I. Introduction

THE scarcity of the radio frequency (RF) spectrum sets a major challenge to the wireless industry as it hinders the persistent efforts of network operators to enhance the capacity and speed of wireless networks. The lighting industry, on the other hand, is actively seeking opportunities to add more value to new illumination devices that utilize light-emitting diodes (LEDs). Compared to traditional incandescent or florescent lamps, LED-based lamps are more reliable and have a longer lifespan, which makes the manufacture and retail of LED-based luminaires a less profitable business in the long run.

Being at the intersection of communication and illumination, visible light communication (VLC) fulfills the needs of both the wireless and lighting industries as it turns illumination devices into wireless data transmitters. VLC systems operate over the license-free light spectrum, wherein the data signal is transmitted by means of modulating the output intensity of the LEDs, i.e., via intensity modulation (IM). At the receiver side, direct detection (DD) is applied using simple photodiodes (PDs). Given the ongoing widespread deployment of LED luminaires, VLC can turn such prevalent illumination devices into wireless access points (APs) that provide ubiquitous indoor broadband coverage, including areas in which RF radiation is undesirable or prohibited, such as hospitals and aircrafts [1]. As shown in Fig. 1, a typical VLC AP covers a service area on the order of $1-10$ m^2. This relatively small coverage area allows ultra-dense deployment of the so-called *VLC attocells* [2], which are analogous, but smaller in terms of the coverage area, to *RF femtocells* [3]. As a consequence, the *area spectral efficiency* (ASE) of VLC networks can be significantly increased, and more users can be accommodated within a certain area [4], [5].

Typical lighting systems utilize multiple wide-beam luminaires to provide uniform illumination. From a communications perspective, however, the use of wide-beam luminaires may cause increased interference levels for users in neighboring attocells, especially those at the edges of the attocells wherein the illumination footprints of luminaires from different attocells overlap together. In fact, it has been shown that the degradation in signal-to-interference-plus-noise ratio (SINR) for attocell-edge users can be as high as 30 dB due largely to increased interference [6].

In order to alleviate the performance degradation for attocell-edge users, several works in the literature have considered hybrid RF-VLC systems [7]–[10]. In such systems, the VLC attocells are deployed with non-overlapping footprints, and the gaps are covered with RF femtocells. In other words, users who are beyond the coverage of the VLC attocells are served by RF base stations. Despite its benefits, a hybrid RF-VLC system would suffer from added complexity along with increased handover overhead for users moving across different femtocells/attocells.

A different approach towards interference management for VLC attocells is to use the so-called *coordinated multipoint* (CoMP) transmission schemes, wherein transmitters of different attocells are connected through backbone networks like wired Ethernet or powerline, and design their signals in a collaborative way [6], [11]–[24]. Most of the research on CoMP VLC has focused on the *joint transmission* (JT) scheme in which all the transmitters jointly serve all the users. It removes the barriers between attocells and turns the previously unwanted inter-attocell interference (IAI) into constructive signal components. JT is typically considered in

This work has been supported by the Natural Sciences and Engineering Research Council of Canada (NSERC).

This article has been accepted for publication in a future issue of this journal, but has not been fully edited. Content may change prior to final publication. Citation information: DOI 10.1109/TCOMM.2018.2817222, IEEE Transactions on Communications

the context of beamforming design or frequency allocation among attocells. In [11], pseudo-inverse-based zero forcing (ZF) and ZF dirty-paper coding were proposed for multi-user multiple-input, single-output (MU-MISO) VLC systems, while a generalized-inverse-based ZF scheme was proposed in [12] to maximize the system sum-rate. In addition, ZF block diagonalization precoding was considered for a multi-user multiple-input, multiple-output (MU-MIMO) VLC system in [13]. Besides ZF, linear beamforming schemes that are based on the minimum mean squared error (MMSE) criterion have also been considered in [6], [14]–[16]. Other JT schemes that exploit frequency allocation have been considered in [17], [18].

Despite their superior performance, the implementation of JT schemes brings two major difficulties. First, information exchange among different transmitters should involve not only downlink channel state information (CSI), but also the data symbols intended for each user. This may not be feasible if the backbone network that interconnects the transmitters together is bandlimited. Second, JT requires tight synchronization among transmitters of different attocells in order to ensure that the signals emitted from different luminaires arrive at the intended user simultaneously.

In order to circumvent such difficulties, researchers have considered other CoMP schemes that require lower coordination level among attocells [19]–[25]. Unlike JT, these coordination schemes only require the sharing of CSI among attocells. In addition, symbol-level synchronization among attocells is not required as each user is served only by its assigned attocell. When the attocells are served by single-luminaire transmitters, the coordination can be implemented via adaptively allocating the time [19], frequency [19]–[25], or power resources [23]–[25] among different attocells. Such allocation schemes restrain the resources available to each attocell, and consequently, the overall data rate of the system is reduced.

In this paper, we propose a *coordinated beamforming* (CB) scheme for interference mitigation in downlink multi-cell MU-MISO VLC systems, where different attocells have multi-luminaire transmitters while each receiver has a single PD. The luminaires in each transmitter are modulated independently of each other using separate drivers. The excess degrees of freedom offered by such multiple luminaires allow forming more directive beams towards the intended receivers while minimizing IAI. Among neighboring attocells, downlink CSI is exchanged through the backbone network for the purpose of coordinated beamforming design. Under the premise of perfect CSI, we use the weighted sum mean square error (WSMSE) as the performance measure and jointly design the beamformers for different attocells. We adopt linear beamforming as it entails low implementation complexity. Furthermore, the WSMSE measure enables us to take intra-attocell and inter-attocell interference, as well as the receivers noise, into account. In addition, it allows assigning different priorities to the users. We then utilize robust optimization to extend the beamforming design to the case of imperfect CSI. We note that robust design has been considered recently in single-cell VLC systems [6], [14], [15], but it hitherto has not been considered for multi-cell VLC systems.

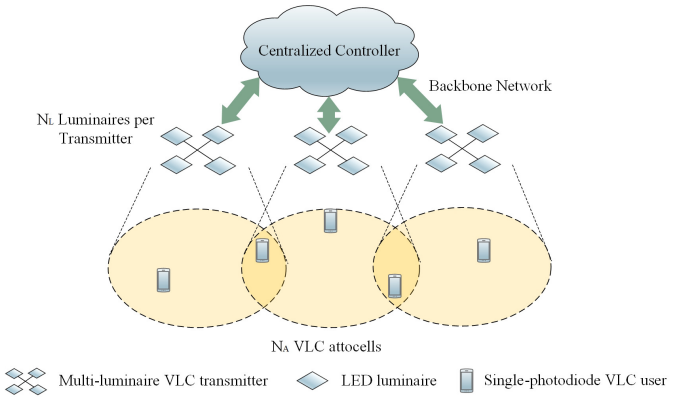

Fig. 1. Illustration of the CB structure.

Unlike the coordination schemes considered in [19]–[23], which are based on time, frequency, or power allocation, our CB scheme exploits the spatial domain for both multiplexing and interference mitigation purposes. In fact, our CB scheme can be integrated with the time and frequency multiplexing techniques considered in [19]–[23] to further enhance the overall system performance. We also note that the concept of CB is not new and has been widely studied for RF channels (see, e.g., [26]–[29]). However, since VLC systems are typically modeled with amplitude constraints on the channel input, the beamforming schemes developed for RF channels are not directly applicable to VLC transmitters.

The remainder of the paper is organized as follows. We introduce the system model and transmission scheme in Section II. In Section III, the design algorithm for CB is proposed assuming perfect downlink CSI at VLC transmitters. In Section IV, the design for CB is extended to the case of imperfect CSI. Numerical results and discussions are provided in Section V, and finally, we conclude the paper in Section VI.

II. Preliminaries

A. Notation

The following notation is adopted throughout the paper. We use $\mathrm{vec}(\cdot)$, $(\cdot)^T$, $(\cdot)^\dagger$, and $(\cdot)^-$ to denote vectorization, transpose, pseudo inverse, and generalized inverse of a matrix, respectively. $\|\cdot\|_p$ represents the p-norm. $\mathcal{R}^{m\times n}$ represents the space of all $m \times n$ matrices with real-valued elements. $\mathrm{diag}(\cdot)$ represents the diagonal matrix whose diagonal elements are obtained from the vector within the parentheses. Expected value is denoted by $\mathbb{E}(\cdot)$. Uppercase bold letters denote matrices, and lowercase bold letters denote vectors.

B. The VLC Channel Model

In this paper, we assume a single-tap VLC channel model. Such an assumption is reasonable when equalization is applied at the transmitter side to flatten the frequency response of the LEDs [30]. Besides, the modulation bandwidth of typical off-the-shelf LED luminaires will not exceed 20 MHz, which is typically smaller than the inverse of the maximum excess delay

This article has been accepted for publication in a future issue of this journal, but has not been fully edited. Content may change prior to final publication. Citation information: DOI 10.1109/TCOMM.2018.2817222, IEEE Transactions on Communications

of the non-LoS (NLoS) path [31]. When the bandwidth of the transmitted signal is below the cutoff frequency of the LED, the overall frequency response of the VLC channel becomes essentially flat.

Without loss of generality, we assume that all the LED luminaires and photodiodes at the users are identical. Assuming the generalized Lambertian emission pattern for the LEDs, the LoS channel gain between an LED luminaire and a user can be approximated as [32]

$$h = \begin{cases} A\cos^m(\phi)\cos(\psi)/D^2 & |\psi| \le \psi_c \ , \\ 0 & |\psi| > \psi_c \ , \end{cases}$$

where m is the Lambertian order that specifies the beam concentration, D is the distance between the LED luminaire and the user, ψ and ϕ are the angles of incidence and irradiance, respectively, ψ_c is the receiver field-of-view (FoV) semi-angle, A is a location-independent coefficient and can be expressed as $A = (m+1)\kappa^2 N_{\rm B} A_{\rm P}\gamma s/(2\pi\sin^2(\phi_c))$, where κ is the concentrator refractive index of the receiver, $N_{\rm B}$ is the number of LED elements per luminaire, $A_{\rm P}$ is the area of photodetector, γ is the photodetector responsivity that represents the light-current conversion efficiency at the receiver, and s is the LED conversion factor that represents the current-light efficiency of the LED at the transmitter.

III. System Model and Transmission Scheme

In this section, we first describe the system model and transmission scheme for the considered multi-cell VLC system. Then the constraints imposed on the linear beamformer are specified to satisfy the amplitude constraints on the transmitted signal.

A. System Model

We consider a downlink VLC system composed of $N_{\rm A}$ coordinated attocells. Each attocell is composed of one VLC transmitter that employs $N_{\rm L}$ LED luminaires. Such luminaires can be modulated independently of each other using separate drivers. The ith attocell serves $N_{\rm U}^i$ single-PD users, and each user is served by a single attocell. The downlink CSI statistics, which is estimated by the user, is fed back to the corresponding VLC transmitter and then shared among different attocells through a bandlimited backbone network.

B. Transmission Scheme

We consider M-ary pulse amplitude modulation (M-PAM) as the modulation scheme, with $M = 2, 4, 8, 16, \ldots$. Let $d_{i_k} \in \{-1, \frac{3-M}{M-1}, \frac{5-M}{M-1}, \ldots, 1\}$, $i = 1, \ldots, N_{\rm A}$, $k = 1, \ldots, N_{\rm U}^i$, denote the data symbol (before DC biasing) intended for the kth user in the ith attocell, and let $\boldsymbol{d}_i = [d_{i_1}, \ldots, d_{i_{N_{\rm U}^i}}]^T$ denote the vector of data symbols intended for all the users in the ith attocell. Note that the entries of $\boldsymbol{d}_i$ are independent, and thus the covariance matrix of $\boldsymbol{d}_i$ is $\eta^2\boldsymbol{I}$, where $\boldsymbol{I}$ represents the identity matrix and

$$\eta = \sqrt{\frac{M+1}{3(M-1)}} \ . \tag{1}$$

Using linear beamforming, the transmitted signal vector at the ith attocell is constructed as

$$\boldsymbol{x}_i = \boldsymbol{F}_i\boldsymbol{d}_i + \boldsymbol{I}_{\rm DC}^i \ , \tag{2}$$

where $\boldsymbol{F}_i \in \mathcal{R}^{N_{\rm L}\times N_{\rm U}^i}$ is the beamforming matrix, and $\boldsymbol{I}_{\rm DC}^i = [I_{\rm DC}^{i_1}, I_{\rm DC}^{i_2}, \cdots, I_{\rm DC}^{i_{N_{\rm L}}}]^T$ is a DC term that sets the illumination level. Note that the the zero-mean nature of the data vector $\boldsymbol{d}_i$ ensures that the illumination level is unaffected by data transmission. For the kth user in the ith attocell u_{i_k}, the received signal can be decomposed into three parts:

1) Intra-attocell Signal: We use $y_{i_k}^{\rm intra}$ to represent the signal component generated within the ith attocell and it is given by

$$\begin{aligned} y_{i_k}^{\rm intra} &= \boldsymbol{h}_{i_k i}^T\boldsymbol{x}_i \\ &= \boldsymbol{h}_{i_k i}^T\mathbf{f}_i^k d_{i_k} + \boldsymbol{h}_{i_k i}^T \sum_{m=1, m\neq k}^{N_{\rm U}^i} \mathbf{f}_i^m d_{i_m} + \boldsymbol{h}_{i_k i}^T\boldsymbol{I}_{\rm DC}^i \ , \end{aligned} \tag{3}$$

where $\boldsymbol{h}_{i_k j} \in \mathcal{R}^{N_{\rm L}\times 1}$ denotes the channel gain vector between u_{i_k} and the VLC transmitter of the jth attocell, and $\mathbf{f}_i^k$ is the kth column vector of $\boldsymbol{F}_i$.

2) Inter-attocell Interference: Besides the intra-attocell signal, user u_{i_k} also receives interfering signals from neighboring attocells. The total interfering signal from all the other attocells $y_{i_k}^{\rm inter}$ can be expressed as

$$\begin{aligned} y_{i_k}^{\rm inter} &= \sum_{j=1, j\neq i}^{N_{\rm A}} \boldsymbol{h}_{i_k j}^T\boldsymbol{x}_j \\ &= \sum_{j=1, j\neq i}^{N_{\rm A}} \sum_{m=1}^{N_{\rm U}^j} \boldsymbol{h}_{i_k j}^T\mathbf{f}_j^m d_{j_m} + \sum_{j=1, j\neq i}^{N_{\rm A}} \boldsymbol{h}_{i_k j}^T\boldsymbol{I}_{\rm DC}^j \ . \end{aligned} \tag{4}$$

3) Receiver noise: The dominant noise at user u_{i_k}, denoted as n_{i_k}, comprises thermal noise generated by the receiver electronic circuits, and shot noise due to ambient illumination. n_{i_k} can be modelled as a zero-mean Gaussian random variable with variance [33]

$$\sigma_{i_k}^2 = \sigma_{\rm th}^2 + 2eB(I_{i_k} + I_{\rm bg}I_2) \ , \tag{5}$$

where $\sigma_{\rm th}^2$ is the thermal-noise variance, e is the elementary charge, B is the VLC system bandwidth, $I_{\rm bg}$ is the background current, I_2 is the noise bandwidth factor (second Personick integral [24]), I_{i_k} is the average current of the received signal at user u_{i_k}, and it can be calculated as

$$I_{i_k} = \sum_{j=1}^{N_{\rm A}} \boldsymbol{h}_{i_k j}^T\boldsymbol{I}_{\rm DC}^j \ . \tag{6}$$

Note that the receiver noise power is dependent on the illumination level and user location via I_{i_k}.

The total received signal $\hat{y}_{i_k}$ at user u_{i_k} is the sum of the three components mentioned above, and can be expressed as Eq. (7). At the receiver, the DC component $\sum_{j=1}^{N_{\rm A}} \boldsymbol{h}_{i_k j}^T\boldsymbol{I}_{\rm DC}^j$ is removed via AC coupling, leaving the information-carrying signal at u_{i_k} as

$$y_{i_k} = \hat{y}_{i_k} - \sum_{j=1}^{N_{\rm A}} \boldsymbol{h}_{i_k j}^T\boldsymbol{I}_{\rm DC}^j \ . \tag{8}$$

This article has been accepted for publication in a future issue of this journal, but has not been fully edited. Content may change prior to final publication. Citation information: DOI 10.1109/TCOMM.2018.2817222, IEEE Transactions on Communications

$$\hat{y}_{i_k} = y_{i_k}^{\text{intra}} + y_{i_k}^{\text{inter}} + n_{i_k} = \underbrace{\boldsymbol{h}_{i_k i}^T \mathbf{f}_i^k d_{i_k}}_{\text{desired signal}} + \underbrace{\boldsymbol{h}_{i_k i}^T \sum_{m=1, m\neq k}^{N_{\text{U}}^i} \mathbf{f}_i^m d_{i_m}}_{\text{intra-attocell interference}} + \underbrace{\sum_{j=1, j\neq i}^{N_{\text{A}}} \sum_{m=1}^{N_{\text{U}}^j} \boldsymbol{h}_{i_k j}^T \mathbf{f}_j^m d_{j_m}}_{\text{inter-attocell interference}} + \underbrace{\sum_{j=1}^{N_{\text{A}}} \boldsymbol{h}_{i_k j}^T \boldsymbol{I}_{\text{DC}}^j}_{\text{DC photocurrent}} + \underbrace{n_{i_k}}_{\text{noise}} \tag{7}$$

C. Design Constraints

For the illumination uniformity of indoor environment, we shall assume that all the LEDs are driven by equal DC bias, i.e.,

$$I_{\text{DC}}^{i_k} = I_{\text{DC}}, \ \forall i, k \tag{9}$$

For typical current-driven LEDs, though the inherent nonlinear current to optical intensity characteristic of LEDs can be compensated by pre-distorters, the dynamic range of LEDs is limited. To ensure that the LED operates within its dynamic range and to avoid clipping, the beamforming matrix $\boldsymbol{F}_i$ must satisfy the constraint [6]

$$\|\boldsymbol{f}_i^k\|_1 \leq \min\left(I_{\text{DC}} - I_{\text{L}}, I_{\text{U}} - I_{\text{DC}}\right), \ \forall i, k, \tag{10}$$

where $\boldsymbol{f}_i^k$ represents the kth row in $\boldsymbol{F}_i$, and $I_{\text{U}} > I_{\text{L}} > 0$ represent the upper and the lower bound of the LED drive current in the linear region.

IV. Beamforming Design with Perfect Channel Information

We consider linear minimum mean square error (MMSE) beamforming design in this paper. Linear beamformers can achieve reasonable throughput performance with lower implementation complexity relative to its nonlinear counterparts [34]. Two major linear beamforming techniques are ZF beamforming and MMSE beamforming. ZF beamforming cancels out multi-user interference through channel inversion. However, ZF is infeasible when the number of luminaries in each attocell is less than the total number of users of all the coordinated attocells [27]. Furthermore, ZF has relatively poor performance in low signal-to-noise ratio region [35]. In comparison, MMSE beamforming has less strict requirement on the number of luminaires per attocell, and outperforms ZF beamforming in noise-limited scenarios as it also takes into account the receiver noise in design optimization [36].

We consider a linear receiver at the VLC user, so the estimated received signal $\hat{d}_{i_k}$ at u_{i_k} can be expressed as

$$\hat{d}_{i_k} = c_{i_k} y_{i_k} \ . \tag{11}$$

where the scaling factor c_{i_k} is the receive filter for user u_{i_k}. Then the mean square error (MSE) for user u_{i_k} can be calculated as

$$\begin{aligned} \text{MSE}_{i_k} &= \mathbb{E}_{\boldsymbol{d},\boldsymbol{n}} \|\hat{d}_{i_k} - d_{i_k}\|_2^2 \qquad (12) \\ &= \eta^2 \|c_{i_k} \boldsymbol{h}_{i_k i}^T \boldsymbol{F}_i - \boldsymbol{e}_{i_k}^T\|_2^2 + \eta^2 \sum_{j=1, j\neq i}^{N_{\text{A}}} \|c_{i_k} \boldsymbol{h}_{i_k j}^T \boldsymbol{F}_j\|_2^2 + c_{i_k}^2 \sigma_{i_k}^2, \end{aligned}$$

where $\boldsymbol{e}_{i_k}$ is the kth standard basis vector for the N_{U}^i-dimensional space with $\boldsymbol{e}_{i_k} = [\mathbf{0}_{1\times(k-1)} \quad 1 \quad \mathbf{0}_{1\times(N_{\text{U}}^i - k)}]^T$. Note that the second term results from the inter-attocell interference and is absent in the MSE expression of JT [6, (30)]. In this section, we aim at optimizing the system performance subject to the LED dynamic range constraint (10) assuming the availability of perfect CSI at the transmitters. We use the WSMSE as the performance measure so that the possibly different priorities of different users can be considered in system design. More specifically,

$$\text{WSMSE} = \sum_{i=1}^{N_{\text{A}}} \text{WSMSE}_i = \sum_{i=1}^{N_{\text{A}}} \sum_{k=1}^{N_{\text{U}}^i} w_{i_k} \text{MSE}_{i_k} \tag{13}$$

where WSMSE_i represents the WSMSE of the ith attocell, and $w_{i_k} > 0$ denotes the priority (weight) of user u_{i_k} at the current scheduling slot according to some criteria. Considering the constraint Eq. (10) on the beamforming matrix, the WSMSE minimization problem can be formulated as

$$\begin{aligned} \text{P1}: \min_{\{\boldsymbol{F}_i\}, \{c_{i_k}\}} \ & \text{WSMSE} \qquad (14) \\ \text{s.t.}: \ & \|\boldsymbol{f}_i^k\|_1 \leq \min\left(I_{\text{DC}} - I_{\text{L}}, I_{\text{U}} - I_{\text{DC}}\right), \ \forall i, k \ . \end{aligned}$$

When w_{i_k} remains the same for all i and k, P1 degenerates to the sum-MSE optimization problem which may impose unfairness across users. More generally, the weights w_{i_k} can be updated over time to maintain fairness among terminals [37]. Designing the optimal weights for the system is outside the scope of the paper. Instead, we focus on obtaining the solution to the optimization problem for a given set of weights. The objective function in optimization problem P1 is biconvex in terms of beamforming matrices $\{\boldsymbol{F}_i\}$ and scaling factors $\{c_{i_k}\}$ [38]. Fixing either of these two groups of variables will result in a (convex) quadratic optimization problem. Here we use the alternating optimization method to, possibly suboptimally, solve the problem. Fixing beamforming matrices $\{\boldsymbol{F}_i\}$, we can obtain the closed-form expression for the optimal MMSE receiving filter

$$c_{i_k}^* = \frac{\eta^2 \boldsymbol{h}_{i_k i}^T \mathbf{f}_i^k}{\eta^2 \sum_{j=1}^{N_{\text{A}}} \sum_{m=1}^{N_{\text{U}}^j} \|\boldsymbol{h}_{i_k j}^T \mathbf{f}_j^m\|_2^2 + \sigma_{i_k}^2}, \forall i, k. \tag{15}$$

We also need to acquire the optimal beamforming matrices $\{\boldsymbol{F}_i\}$ given fixed scaling factors $\{c_{ik}\}$. For notational simplicity, we define

$$\begin{aligned} \boldsymbol{H}_{ij} &= [\boldsymbol{h}_{i_1 j}, \boldsymbol{h}_{i_2 j}, \ldots, \boldsymbol{h}_{i_{N_{\text{U}}^i} j}]^T, \\ \boldsymbol{C}_i &= \text{diag}([c_{i_1}, c_{i_2}, \cdots, c_{i_{N_{\text{U}}^i}}]^T), \\ \boldsymbol{W}_i &= \text{diag}([\sqrt{w_{i_1}}, \sqrt{w_{i_2}}, \cdots, \sqrt{w_{i_{N_{\text{U}}^i}}}]^T), \\ \boldsymbol{n}_i &= [n_{i_1}, n_{i_2}, \ldots, n_{i_{N_{\text{U}}^i}}]^T. \end{aligned}$$

Then WSMSE_i can be expressed as Eq. (16). Define $\boldsymbol{w}_i =$

This article has been accepted for publication in a future issue of this journal, but has not been fully edited. Content may change prior to final publication. Citation information: DOI 10.1109/TCOMM.2018.2817222, IEEE Transactions on Communications

$\mathrm{vec}\,(\boldsymbol{W}_i)$, $\boldsymbol{A}_{ij} = (\boldsymbol{W}_i \boldsymbol{C}_i \boldsymbol{H}_{ij}) \otimes \boldsymbol{I}$, $\boldsymbol{f}_j = \mathrm{vec}\big(\boldsymbol{F}_j^T\big)$, and $\boldsymbol{V}_i$ as the $N_{\mathrm{L}} N_{\mathrm{U}}^i \times N_{\mathrm{U}}^i N_{\mathrm{L}}$ block-diagonal matrix of the $N_{\mathrm{L}} \times N_{\mathrm{U}}^i$ all-one matrix. With fixed $\{c_{i_k}\}$, P1 can be transformed into

$$\begin{aligned} \mathrm{P2}: \min_{\{\boldsymbol{f}_i\}} \; & \sum_{i=1}^{N_{\mathrm{A}}} \Big(\eta^2 \left\| \boldsymbol{A}_{ii} \boldsymbol{f}_i - \boldsymbol{w}_i \right\|_2^2 + \eta^2 \sum_{j=1, j\neq i}^{N_{\mathrm{A}}} \left\| \boldsymbol{A}_{ij} \boldsymbol{f}_j \right\|_2^2 \\ & + \sum_{k=1}^{N_{\mathrm{U}}^i} w_{i_k}^2 c_{i_k}^2 \sigma_{i_k}^2 \Big) \qquad (17) \\ \text{s.t.} \quad & -\boldsymbol{t}_i \leq \boldsymbol{f}_i \leq \boldsymbol{t}_i, \; \forall i \; , \\ & \boldsymbol{V}_i \boldsymbol{t}_i \leq \min\left(I_{\mathrm{DC}} - I_{\mathrm{L}}, I_{\mathrm{U}} - I_{\mathrm{DC}}\right) \mathbf{1}_{N_{\mathrm{L}} N_{\mathrm{U}}^i \times 1}, \; \forall i \; . \end{aligned}$$

P2 is a convex quadratic programming problem and can be efficiently solved by the MOSEK solver [39]. Once P2 is solved, the optimal beamforming matrices $\boldsymbol{F}_j$ can be retrieved from vector $\boldsymbol{f}_j$.

For the suboptimal alternating optimization, the ZF beamformer can be used as the initialization point. Define the concatenation of all channel matrices as

$$\boldsymbol{H} = [\boldsymbol{H}_{11}^T, \ldots, \boldsymbol{H}_{N_{\mathrm{A}}1}^T, \ldots, \boldsymbol{H}_{1N_{\mathrm{A}}}^T, \ldots, \boldsymbol{H}_{N_{\mathrm{A}}N_{\mathrm{A}}}^T].$$

When $N_{\mathrm{L}} \geq \sum_{i=1}^{N_{\mathrm{A}}} N_{\mathrm{U}}^i$, the general form for the transmit ZF beamformer of the ith attocell can be expressed as [27]:

$$\begin{aligned} \boldsymbol{F}_i^{\mathrm{ZF}} &= \Big(\sum_{j=1}^{N_{\mathrm{A}}} \sum_{m=1}^{N_{\mathrm{A}}} \sum_{k=1}^{N_{\mathrm{U}}^j} \boldsymbol{h}_{j_k m} \boldsymbol{h}_{j_k m}^T \Big)^{-} \boldsymbol{H}_{ii}^T \, \mathrm{diag}(\boldsymbol{\Lambda}_i) \qquad (18) \\ &= \big(\boldsymbol{H}\boldsymbol{H}^T\big)^{-} \boldsymbol{H}_{ii}^T \, \mathrm{diag}(\boldsymbol{\Lambda}_i) \; , \end{aligned}$$

where

$$\begin{aligned} \boldsymbol{\Lambda}_i &= [\Lambda_{i_1}, \Lambda_{i_2}, \ldots, \Lambda_{i_{N_{\mathrm{U}}^i}}]^T \; , \\ \big(\boldsymbol{H}\boldsymbol{H}^T\big)^{-} &= \big(\boldsymbol{H}\boldsymbol{H}^T\big)^{\dagger} + \big(\boldsymbol{I} - \big(\boldsymbol{H}\boldsymbol{H}^T\big)^{\dagger} \big(\boldsymbol{H}\boldsymbol{H}^T\big) \boldsymbol{U}_i\big) \; . \end{aligned}$$

$\Lambda_{i_k} > 0$ represents the symbol gain for d_{i_k}, and $\boldsymbol{U}_i$ is an arbitrary matrix. Then we have

$$\boldsymbol{H}_{ji} \boldsymbol{F}_i^{\mathrm{ZF}} = \begin{cases} \boldsymbol{0} & i \neq j \; , \\ \mathrm{diag}(\boldsymbol{\Lambda}_i) & i = j \; . \end{cases}$$

In this paper, we set

$$\begin{aligned} \boldsymbol{U}_i &= \big(\boldsymbol{H}\boldsymbol{H}^T\big)^{\dagger} \big(\boldsymbol{H}\boldsymbol{H}^T\big) \; , \\ \boldsymbol{\Lambda}_i &= \frac{\min\left(I_{\mathrm{DC}} - I_{\mathrm{L}}, I_{\mathrm{U}} - I_{\mathrm{DC}}\right)}{\max_m \left(\sum_{k=1}^{N_{\mathrm{U}}^i} \left| \left(\left(\boldsymbol{H}\boldsymbol{H}^T \right)^{\dagger} \boldsymbol{H}_{ii}^T \right)_{m,k} \right| \right)} \mathbf{1}_{N_{\mathrm{U}}^i \times 1} \; , \end{aligned}$$

and we get

$$\boldsymbol{F}_i^{\mathrm{ZF}} = \left(\boldsymbol{H}\boldsymbol{H}^T \right)^{\dagger} \boldsymbol{H}_{ii}^T \, \mathrm{diag}(\boldsymbol{\Lambda}_i) \; . \qquad (19)$$

Such a ZF beamforming matrix satisfies the constraint of P1 and can be used as the initialization point for the alternating optimization algorithm. We note that when $N_{\mathrm{L}} < \sum_{i=1}^{N_{\mathrm{A}}} N_{\mathrm{U}}^i$, the inter-attocell and intra-attocell interference can not be fully canceled with the beamforming matrix (19). However, (19) still remains a wise choice for the initialization purpose [27]. The algorithm for solving P1 is summarized in Algorithm 1.

Algorithm 1 Alternating optimization algorithm for P1

1. **Initialization**:
   $p \Leftarrow 0$.
   Update $\boldsymbol{H}_{ij}$ with CSI.
   Initialize $\{\boldsymbol{F}_i\}$.
2. **repeat**
3. Update $\{c_{i_k}\}$ according to Eq. (15).
4. Update $\{\boldsymbol{A}_{ij}\}$ with $\{c_{i_k}\}$.
5. Solve P2 and get $\{\boldsymbol{F}_i\}$.
6. $p \Leftarrow p + 1$.
7. **until** $\|\mathrm{WSMSE}^{p+1} - \mathrm{WSMSE}^p\| \leq \delta$ (δ is a predefined threshold) or $p = p_{\max}$ ($p_{\max}$ is a predefined maximum iteration number).

V. Robust Beamforming Design with Channel Uncertainty

The linear beamforming design in the previous section is based on the premise of perfect CSI. In practice, however, CSI at the transmitter side is usually contaminated due to various factors like quantization, erroneous channel estimation or outdated feedback. Assuming an additive channel uncertainty model, the actual channel gain can be expressed as

$$\boldsymbol{h}_{i_k j} = \hat{\boldsymbol{h}}_{i_k j} + \boldsymbol{\delta}_{i_k j} \; , \qquad (20)$$

where $\hat{\boldsymbol{h}}_{i_k j}$ represents the channel estimate, $\boldsymbol{\delta}_{i_k j}$ represents the error vector resulting from channel uncertainty. As a result, the MSE for user u_{i_k} can be expressed as

$$\begin{aligned} \mathrm{MSE}_{i_k} = \; & \eta^2 \| c_{i_k} (\hat{\boldsymbol{h}}_{i_k i}^T + \boldsymbol{\delta}_{i_k i}^T) \boldsymbol{F}_i - \boldsymbol{e}_k^T \|_2^2 \\ & + \eta^2 \sum_{j=1, j\neq i}^{N_{\mathrm{A}}} \| c_{i_k} (\hat{\boldsymbol{h}}_{i_k j}^T + \boldsymbol{\delta}_{i_k j}^T) \boldsymbol{F}_j \|_2^2 + c_{i_k}^2 \sigma_{i_k}^2 \; . \end{aligned}$$

Typically, there are two classes of models to characterize $\boldsymbol{\delta}_{i_k j}$: the *deterministic* model and the *stochastic* model. For the deterministic model, we assume the actual channel gain vector, although not exactly known, lies within a certain region with the estimated nominal value at the center of the region. In this paper, we assume $\|\boldsymbol{\delta}_{i_k j}\| \leq \epsilon$, where ϵ is some known constant and represents the level of uncertainty[1]. The goal of robust design with the deterministic model is to guarantee a certain performance level for every possible channel realizations, which is achieved through optimizing the worst-case performance by solving a min-max optimization problem [40], [41]. For the stochastic model, we model the elements of error vector $\boldsymbol{\delta}_{i_k j}$ as Gaussian distributed random variables. Particularly in this paper, we assume $\boldsymbol{\delta}_{i_k j}$ is zero-mean Gaussian distributed with covariance matrix $\sigma_e^2 \boldsymbol{I}$, where σ_e is some known constant. With the stochastic model, we aim at optimizing the average performance over the error vector, which guarantees a system performance averaged over possible error realizations [40], [41]. Compared with the non-robust design proposed in Section IV, robust beamforming

[1]We assume the same level of CSI uncertainty for each user in this paper.

This article has been accepted for publication in a future issue of this journal, but has not been fully edited. Content may change prior to final publication. Citation information: DOI 10.1109/TCOMM.2018.2817222, IEEE Transactions on Communications

$$\mathrm{WSMSE}_i = \sum_{k=1}^{N_{\mathrm{U}}^i} w_{i_k} \mathrm{MSE}_{i_k} = \mathbb{E}_{\boldsymbol{d},\boldsymbol{n}_i}\Big\{ \Big\| \boldsymbol{W}_i \Big(\boldsymbol{C}_i \big(\sum_{j=1}^{N_{\mathrm{A}}} \boldsymbol{H}_{ij} \boldsymbol{F}_j \boldsymbol{d}_j + \boldsymbol{n}_i \big) - \boldsymbol{d}_i \Big) \Big\|_2^2 \Big\} \tag{16}$$

$$= \eta^2 \Big\| \big((\boldsymbol{W}_i \boldsymbol{C}_i \boldsymbol{H}_{ii}) \otimes \boldsymbol{I} \big) \mathrm{vec}\left(\boldsymbol{F}_i^T \right) - \mathrm{vec}\left(\boldsymbol{W}_i \right) \Big\|_2^2 + \eta^2 \sum_{j=1, j\neq i}^{N_{\mathrm{A}}} \Big\| \big((\boldsymbol{W}_i \boldsymbol{C}_i \boldsymbol{H}_{ij}) \otimes \boldsymbol{I} \big) \mathrm{vec}\left(\boldsymbol{F}_j^T \right) \Big\|_2^2 + \sum_{k=1}^{N_{\mathrm{U}}^i} w_{i_k}^2 c_{i_k}^2 \sigma_{i_k}^2$$

design problems are more involved to solve due to the presence of the error vector. However, as will be shown in Section VI.D, robust beamforming is able to mitigate performance degradation due to imperfect CSI, which is highly desirable for practical applications. We note that similar robust designs for both the error models above have recently been considered in single-cell VLC systems [6], [14], [15]. However, it is applied here for the first time for multi-cell VLC systems.

A. Robust Design with the Deterministic Model

In this subsection, we apply the deterministic model to characterize the CSI imperfection and aim at ensuring worst-case robustness through beamforming design. P1 is modified to the min-max optimization problem

$$\begin{aligned} \mathrm{P3}: \min_{\{\boldsymbol{F}_i\},\{c_{i_k}\}} \max_{\|\boldsymbol{\delta}_{i_k j}\|_2 \le \epsilon} \mathrm{WSMSE} &= \sum_{i=1}^{N_{\mathrm{A}}} \sum_{k=1}^{N_{\mathrm{U}}^i} w_{i_k} \mathrm{MSE}_{i_k} \\ \text{s.t.}: \|\boldsymbol{f}_i^k\|_1 &\le \min\left(I_{\mathrm{DC}} - I_{\mathrm{L}}, I_{\mathrm{U}} - I_{\mathrm{DC}} \right), \ \forall i, k \ , \end{aligned}$$

Using the Schur complement lemma [42] and [43, Lemma 2], P3 can be transformed into

$$\begin{aligned} \mathrm{P4}: \min_{\{\boldsymbol{F}_i\},\{\boldsymbol{c}_i\},\{\eta_{i_k j}\},\{t_{i_k j}\},\{g_{i_k}\}} & z^2 \\ \text{s.t.} \quad & \|\boldsymbol{f}_i^k\|_1 \le \min\left(I_{\mathrm{DC}} - I_{\mathrm{L}}, I_{\mathrm{U}} - I_{\mathrm{DC}} \right), \ \forall i, k \ , \\ & \boldsymbol{\Psi}_{i_k j} \succeq 0, \ \forall i, j, k \ , \\ & \boldsymbol{\Phi}_{i_k} \succeq 0, \ \forall i, k \ , \\ & \eta_{i_k j} \ge 0, \ \forall i, j, k \ , \\ & \boldsymbol{\kappa} \succeq 0, \end{aligned} \tag{21}$$

where $\boldsymbol{\Psi}_{i_k j}$ is expressed in (22), and

$$\boldsymbol{\kappa} = \begin{bmatrix} z & \boldsymbol{\omega}^T \\ \boldsymbol{\omega} & z\boldsymbol{I} \end{bmatrix},$$

$$\boldsymbol{\Phi}_{i_k} = \begin{bmatrix} g_{i_k} & t_{i_k 1} & \dots & t_{i_k N_{\mathrm{A}}} & c_{i_k}\sigma_{i_k} \\ t_{i_k 1} & & & & \\ \vdots & & & g_{i_k}\boldsymbol{I} & \\ t_{i_k N_{\mathrm{A}}} & & & & \\ c_{i_k}\sigma_{i_k} & & & & \end{bmatrix},$$

$$\boldsymbol{\omega} = [w_{1_1} g_{1_1}, \dots, w_{1_{N_{\mathrm{U}}^1}} g_{1_{N_{\mathrm{U}}^1}}, \dots, w_{N_{\mathrm{A}}{}_{N_{\mathrm{U}}^{N_{\mathrm{A}}}}} g_{N_{\mathrm{A}}{}_{N_{\mathrm{U}}^{N_{\mathrm{A}}}}}]^T \ .$$

Similar to Algorithm 1 for P1, a local optimum of P4 can be obtained through alternatively optimizing over $\{\boldsymbol{F}_i\}$ and $\{\boldsymbol{c}_i\}$. Each problem is an SDP and can be solved numerically.

B. Robust Design with the Stochastic Model

For the stochastic error model, we would like to secure the average system performance in the robust design. The optimization problem can be formulated as

$$\begin{aligned} \mathrm{P5}: \min_{\{\boldsymbol{F}_i\},\{c_{i_k}\}} \mathbb{E}_{\boldsymbol{\delta}_{i_k j}} \left(\mathrm{WSMSE} \right) &= \sum_{i=1}^{N_{\mathrm{A}}} \sum_{k=1}^{N_{\mathrm{U}}^i} w_{i_k} \mathbb{E}_{\boldsymbol{\delta}_{i_k j}} \left(\mathrm{MSE}_{i_k} \right) \\ \text{s.t.}: \|\boldsymbol{f}_i^k\|_1 &\le \min\left(I_{\mathrm{DC}} - I_{\mathrm{L}}, I_{\mathrm{U}} - I_{\mathrm{DC}} \right), \ \forall i, k \ . \end{aligned} \tag{23}$$

Alternating optimization can also be used to solve P5 which is a non-convex optimization problem. Fixing $\{c_{i_k}\}$, P5 can be transformed into

$$\begin{aligned} \mathrm{P6}: \min_{\{\boldsymbol{F}_i\}} \ & \sum_{i=1}^{N_{\mathrm{A}}} \Big(\eta^2 \Big\| \hat{\boldsymbol{A}}_{ii} \boldsymbol{f}_i - \boldsymbol{w}_i \Big\|_2^2 + \sum_{j=1, j\neq i}^{N_{\mathrm{A}}} \eta^2 \Big\| \hat{\boldsymbol{A}}_{ij} \boldsymbol{f}_j \Big\|_2^2 \\ & + \mathrm{Tr}(\boldsymbol{W}_i^2 \boldsymbol{C}_i^2) \eta^2 \sigma_e^2 \sum_{j=1}^{N_{\mathrm{A}}} \|\boldsymbol{f}_j\|_2^2 + \sum_{k=1}^{N_{\mathrm{U}}^i} w_{i_k}^2 c_{i_k}^2 \sigma_{n_{i_k}}^2 \Big) \\ \text{s.t.} \quad & -\boldsymbol{t}_i \le \boldsymbol{f}_i \le \boldsymbol{t}_i, \ \forall i \ , \\ & \boldsymbol{V}_i \boldsymbol{t}_i \le \min\left(I_{\mathrm{DC}} - I_{\mathrm{L}}, I_{\mathrm{U}} - I_{\mathrm{DC}} \right) \mathbf{1}_{N_{\mathrm{L}} N_{\mathrm{U}}^i \times 1}, \ \forall i \ . \end{aligned}$$

where

$$\hat{\boldsymbol{A}}_{ij} = \Big(\boldsymbol{W}_i \boldsymbol{C}_i \hat{\boldsymbol{H}}_{ij} \Big) \otimes \boldsymbol{I},$$

$$\hat{\boldsymbol{H}}_{ij} = \Big[\hat{\boldsymbol{h}}_{i_1 j}, \hat{\boldsymbol{h}}_{i_2 j}, \dots, \hat{\boldsymbol{h}}_{i_{N_{\mathrm{U}}^i} j} \Big]^T \ .$$

P6 is a convex quadratic programming problem and can be solved numerically. Fixing $\{\boldsymbol{F}_i\}$, we have

$$c_{i_k}^* = \frac{\eta^2 \hat{\boldsymbol{h}}_{i_k i}^T \mathbf{f}_i^k}{\eta^2 \sum_{j=1}^{N_{\mathrm{A}}} \sum_{m=1}^{N_{\mathrm{U}}^j} (\|\hat{\boldsymbol{h}}_{i_k m}^T \mathbf{f}_j^m\|_2^2 + \sigma_e^2 \|\mathbf{f}_j^m\|_2^2) + \sigma_{i_k}^2}, \forall i, k.$$

VI. Simulation Results and Discussions

In this section, we present our simulation results to demonstrate the performance of the proposed CB scheme. First, we compare the performance of VLC systems under different coordination schemes. Then we show that a careful choice of the weighting vector can significantly improve fairness among users. Finally, we demonstrate the performance gain of the adopted robust beamforming design given imperfect CSI.

A. Simulation Setup

We consider on-off keying (OOK) as the modulation scheme for the simulation, i.e., $M = 2$, and thus $\eta = 1$. This is perhaps the most practical transmission scheme for IM systems

This article has been accepted for publication in a future issue of this journal, but has not been fully edited. Content may change prior to final publication. Citation information: DOI 10.1109/TCOMM.2018.2817222, IEEE Transactions on Communications

$$\boldsymbol{\Psi}_{i_k j} = \begin{cases} \begin{bmatrix} t_{i_k i} - \eta_{i_k i} & \eta(c_{i_k} \hat{\boldsymbol{h}}_{i_k i}^T \boldsymbol{F}_i - \boldsymbol{e}_k^T) & \mathbf{0} \\ \eta(c_{i_k} (\hat{\boldsymbol{h}}_{i_k i}^T \boldsymbol{F}_i)^T - \boldsymbol{e}_k) & t_{i_k i} \boldsymbol{I} & \epsilon\eta c_{i_k} \boldsymbol{F}_i^T \\ \mathbf{0} & \epsilon\eta c_{i_k} \boldsymbol{F}_i & \eta_{i_k i} \boldsymbol{I} \end{bmatrix} & i = j \ , \\ \begin{bmatrix} t_{i_k j} - \eta_{i_k j} & \eta c_{i_k} \hat{\boldsymbol{h}}_{i_k j}^T \boldsymbol{F}_j & \mathbf{0} \\ \eta c_{i_k} (\hat{\boldsymbol{h}}_{i_k j}^T \boldsymbol{F}_j)^T & t_{i_k j} \boldsymbol{I} & \epsilon\eta c_{i_k} \boldsymbol{F}_j^T \\ \mathbf{0} & \epsilon\eta c_{i_k} \boldsymbol{F}_j & \eta_{i_k j} \boldsymbol{I} \end{bmatrix} & i \neq j \ . \end{cases} \tag{22}$$

$$\mathrm{SINR}_{i_k} = \frac{\eta^2 \| \boldsymbol{h}_{i_k i}^T \mathbf{f}_i^k \|^2}{\eta^2 \sum_{j=1, j\neq k}^{N_{\mathrm{U}}^i} \| \boldsymbol{h}_{i_k i}^T \mathbf{f}_i^j \|^2 + \eta^2 \sum_{j=1, j\neq i}^{N_{\mathrm{A}}} \sum_{m=1}^{N_{\mathrm{U}}^j} \| \boldsymbol{h}_{i_k j}^T \mathbf{f}_j^m \|^2 + \sigma_{i_k}^2} \tag{24}$$

because of simplicity and immunity to nonlinear distortion. We consider an indoor environment illustrated in Fig. 2a for our simulation purposes. The coordinate system and the area planning[2] are both shown in Fig. 2b. The room dimensions are $10 \times 5 \times 3$ m^3. Two multi-luminaire VLC transmitters ($N_{\mathrm{A}} = 2$) are installed in the ceiling and are interconnected through a backbone network. Simulation parameters for VLC transmitters and receivers are listed in Table I. We consider two lighting setups, where $N_{\mathrm{L}} = 2, N_{\mathrm{B}} = 64$ for Lighting Setup I (LS-I) and $N_{\mathrm{L}} = 4, N_{\mathrm{B}} = 36$ for Lighting Setup II (LS-II). The coordinates of LED luminaires in each setup are listed in Table II.

As the primary function of VLC transmitters is illumination, we first investigate the illumination performance of the two lighting setups. For simplicity, we only consider the LoS component of visible light propagation to approximate the indoor illumination performance, where the photometric parameters of LXW8-PW40 Luxeon Rebel high power LEDs are applied for the calculation [45]. The illuminance distribution with LS-I and LS-II are shown in Fig. 3a and Fig. 3b when $I_{\mathrm{DC}} = 500$ mA, respectively. The corresponding average illuminance and uniformity of the task area and the immediate surrounding area under both lighting setups are shown in Table III. According to the European Norm (EN) 12464-1 standard [44], the illuminance and uniformity of both setups satisfy the requirements for office work and study. In this section, we use the SINR as expressed in Eq. (24) as the metric for performance comparison.

If not stated otherwise, we assume $N_{\mathrm{U}}^i = 2, \forall\ i$ in the following[3]. Note that the specific values of the system parameters M, N_{U}^i, N_{A} and N_{L} chosen in this section are solely for the purpose of simulation illustration, and the system design can be applied to any values of M, N_{U}^i, N_{A} and N_{L}.

[2]According to the European Norm (EN) 12464-1 standard [44] for the planning and design of lighting installations, the area planning for indoor workplaces defines both task area and immediate surrounding area. The *task area* is defined as the area in which the visual task is carried out. The *immediate surrounding area* is defined as a band surrounding the task area within the field of vision with a minimum width of 0.5 m.

[3]For $N_{\mathrm{A}} = 2$ and $N_{\mathrm{U}}^i = 2$, LS-I ($N_{\mathrm{L}} = 2$) satisfies $N_{\mathrm{L}} < \sum_{i=1}^{N_{\mathrm{A}}} N_{\mathrm{U}}^i$ while LS-II ($N_{\mathrm{L}} = 4$) satisfies $N_{\mathrm{L}} \geq \sum_{i=1}^{N_{\mathrm{A}}} N_{\mathrm{U}}^i$.

(a) Room Illustration.

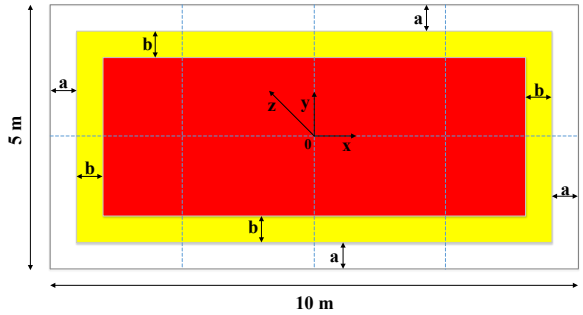

(b) Illustration of office areas. The yellow zone is the immediate surrounding area, and the red area is the task area. $b = 0.5$ m. Illuminance calculations can ignore a marginal strip extending $a = 0.5$ m from the walls according to [44].

Fig. 2. Room Setup.

B. Comparison of Different Coordination Levels

We first investigate the benefit of coordinated transmission for VLC systems. We consider three different coordination levels:

1) *Joint Transmission (JT)*: Both user data and CSI are shared among attocells, and the two attocells essentially merge into one single attocell, and operate together as a single MU-MISO system [6], [11], [14]–[16].
2) *Coordinated Beamforming (CB)*: Different from JT, only CSI is shared among the attocells. Based on the shared channel information, beamforming matrices for different attocells are designed collaboratively to alleviate IAI.
3) *Uncoordinated Transmission (UT)*: Attocells are uncoordinated, and each attocell operates as an independent MU-MISO system when $N_{\mathrm{L}} \geq 2$ and $N_{\mathrm{U}}^i \geq 2$.

This article has been accepted for publication in a future issue of this journal, but has not been fully edited. Content may change prior to final publication. Citation information: DOI 10.1109/TCOMM.2018.2817222, IEEE Transactions on Communications

TABLE I
SIMULATION PARAMETERS

Transmitter Parameters	
I_{L}	300 [mA]
I_{U}	700 [mA]
Lambertian order m	1
LED conversion factor s	0.44 [W/A]
System Bandwidth B	10 [MHz]

Receiver Parameters	
PD area A_{PD}	1 [cm^2]
Concentrator refractive index κ	1.5
Receiver FoV ψ_c	60 [deg.]
Noise bandwidth factor I_2	0.562
Background current I_{bg}	100 [μA]
PD responsivity γ	0.30 [A/W]

TABLE II
LUMINAIRE COORDINATES OF LS-I AND LS-II

Attocell I		Attocell II	
Luminaire 1	[2.5, 1.25, 3]	Luminaire 3	[-2.5, 1.25, 3]
Luminaire 2	[2.5, -1.25, 3]	Luminaire 4	[-2.5, -1.25, 3]

(a) Lighting Setup I (LS-I), $N_{\mathrm{L}} = 2$, $N_{\mathrm{B}} = 64$.

Attocell I		Attocell II	
Luminaire 1	[3, 1.25, 3]	Luminaire 5	[-2, 1.25, 3]
Luminaire 2	[3, -1.25, 3]	Luminaire 6	[-2, -1.25, 3]
Luminaire 3	[2, 1.25, 3]	Luminaire 7	[-3, 1.25, 3]
Luminaire 4	[2, -1.25, 3]	Luminaire 8	[-3, -1.25, 3]

(b) Lighting Setup II (LS-II), $N_{\mathrm{L}} = 4$, $N_{\mathrm{B}} = 36$.

TABLE III
ILLUMINATION PERFORMANCE OF LS-I AND LS-II

LS-I	Illuminance (lx)	Uniformity
task area	624.7	0.604
immediate surrounding area	506.6	0.496

LS-II	Illuminance (lx)	Uniformity
task area	695.6	0.662
immediate surrounding area	571.3	0.527

TABLE IV
USER COORDINATES

Attocell I		Attocell II	
User 1	[x_1, 1.25, 0.8]	User 3	[-2.5, 1.25, 0.8]
User 2	[2.5, -1.25, 0.8]	User 4	[-2.5, -1.25, 0.8]

(a) User Distribution I (UD-I)

Attocell I		Attocell II	
User 1	[0.25, 0.25, 0.8]	User 3	[-0.25, 0.25, 0.8]
User 2	[0.25, -0.25, 0.8]	User 4	[-0.25, -0.25, 0.8]

(b) User Distribution II (UD-II)

Attocell I		Attocell II	
User 1	[0.25, 1.25, 0.8]	User 3	[-0.25, 1.25, 0.8]
User 2	[0.25, -1.25, 0.8]	User 4	[-0.25, -1.25, 0.8]

(c) User Distribution III (UD-III)

Attocell I		Attocell II	
User 1	[0.25, 2.5, 0.8]	User 3	[-0.25, 2.5, 0.8]
User 2	[0.25, -2.5, 0.8]	User 4	[-0.25, -2.5, 0.8]

(d) User Distribution IV (UD-IV)

In this subsection, we consider User Distribution I (UD-I) listed in Table IV. We set $w_{i_k} = 1, \forall i, k$, and thus P1 reduces to a sum-MSE minimization problem. We focus on the area wherein users will suffer from IAI, namely the region of $-2\ \mathrm{m} \leq x \leq 2\ \mathrm{m}$ under our system setup (see Fig. 2b).

The benefit of the CB scheme is demonstrated in Fig. 4. Fig. 4a and Fig. 4b plot the SINR of User 1 as a function of its x-axis coordinate x_1 with LS-I and LS-II, respectively. In Fig. 4a with LS-I, we can observe that JT produces the best performance among the three schemes. As User 1 moves closer to the edge of the neighboring attocell, i.e., x_1 approaches zero, the achievable SINR decreases dramatically due to the increasing interference from neighboring attocell, and the UT scheme suffers the most significant performance degradation due to the lack of coordination. For LS-I with $N_{\mathrm{L}} = 2$, CB provides an intermediate achievable SINR between that of JT and UT. For LS-II with $N_{\mathrm{L}} = 4$, as can be seen from Fig. 4b, the achievable SINR of User 1 with CB is almost the same as that with JT. In comparison to LS-I, LS-II has more transmission power and more degrees of freedom in the beamforming design, thus the resulting beamformer can direct more transmission power onto the targeted user and leak relatively less interference to neighboring users at the same time.

From Fig. 4, it may seem that CB can replace JT as long as N_{L} is large enough. However, CB does have its limitations. In Fig. 5, we consider three user distributions for each lighting setup: UD-II, UD-III and UD-IV as listed in Table IV. The similarity of the three setups is that all users are located at the attocell edge and are close to users in the neighboring attocell. For LS-I, we can observe that JT significantly outperforms CB and UT schemes, and the CB scheme can barely improve the performance to a decent level. For LS-II, while CB can significantly increase the SINR in UD-III, the performance of UD-II still barely improves with CB. An intuitive explanation is that all users in UD-II are closer to each other, making the beamformer difficult to target one user without interfering another one. While for UD-IV, CB provides no improvement compared with UT for both lighting setups. The reason is that each user in UD-IV can only be reached by one single luminaire of its belonging attocell, making interference mitigation through beamforming impossible.

From the above results, we can see that although CB often displays comparable performance with JT, the performance gap between JT and CB may become large with specific user distributions. A possible solution is to apply *Coordinated*

This article has been accepted for publication in a future issue of this journal, but has not been fully edited. Content may change prior to final publication. Citation information: DOI 10.1109/TCOMM.2018.2817222, IEEE Transactions on Communications

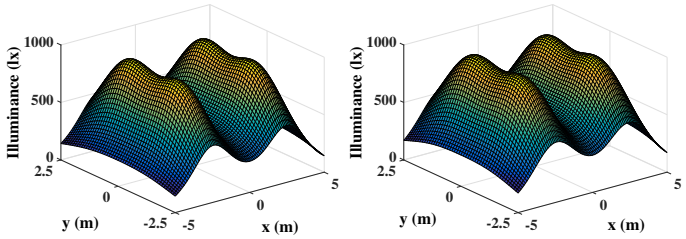

(a) LS-I (b) LS-II

Fig. 3. The distribution of indoor illuminance for two lighting setups when $I_{\mathrm{DC}} = 500$ mA.

Scheduling (CS) jointly with the CB scheme across attocells to make sure that users with such distribution do not get served in the same time slot, so that we can enjoy the architectural benefit of CB while maintaining a comparable performance to JT.

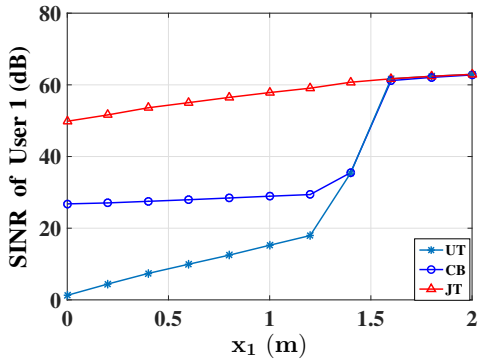

(a) LS-I ($N_{\mathrm{L}} = 2$)

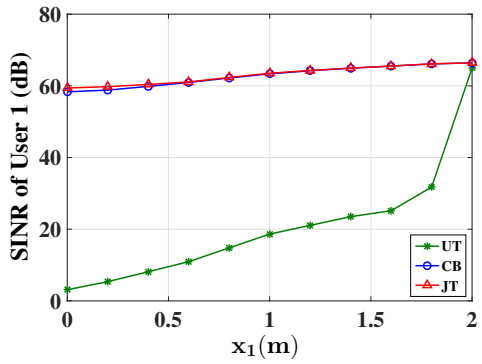

(b) LS-II ($N_{\mathrm{L}} = 4$)

Fig. 4. SINR of User I as a function of its x-axis coordinate x_1.

C. Importance of Weight

Fairness considerations are of particular importance for multiuser VLC systems. Unlike RF wireless communication, indoor VLC channels are free from multipath fading due to the large photodiode size compared with the optical wavelength. Consequently, the deterministic nature of the VLC channel will fix attocell-edge users in low SNR channels for a relatively long time if sum-MSE maximization is the only objective in system optimization. Therefore, the WSMSE design criterion

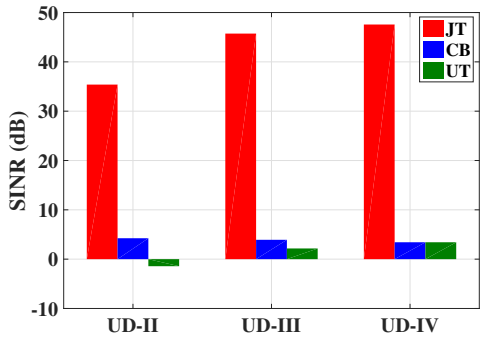

(a) LS-I ($N_{\mathrm{L}} = 2$)

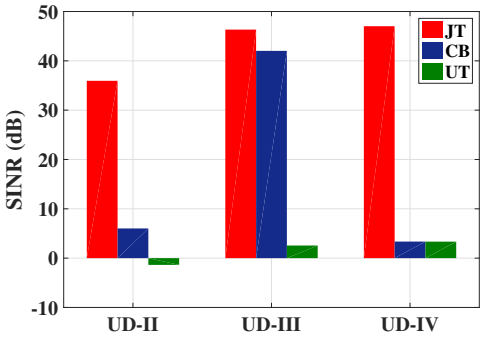

(b) LS-II ($N_{\mathrm{L}} = 4$)

Fig. 5. Comparison of system performance with different coordination levels for UD-II, UD-III and UD-IV.

is a desirable feature to ensure some level of fairness among the users. In the WSMSE optimization problem P1, the weight variable w_{i_k} represents the priority of user u_{i_k}. The weight provides a tradeoff between maximizing the total system throughput and balancing the fairness among users. In this subsection, we consider UD-I with $x_1 = 1$ m and define $\boldsymbol{w} = [w_{1_1}, w_{1_2}, w_{2_1}, w_{2_2}]^T$. When $\boldsymbol{w} = [1,1,1,1]^T$, the user scheduling reduces to sum-MSE minimizing scheduling. The SINR values of 4 users when $\boldsymbol{w} = [1,1,1,1]^T$ are shown in Fig. 6a. We can observe that SINR of User 1 is much lower than the rest of users. This is because the location of User 1 leads to strong inter-attocell interference from Attocell II. User 1 will continuously suffer from low SINR as long as all users remain still. To maintain a level of fairness across users, we can adjust the weights of the users. For example, the SINR plot when $\boldsymbol{w} = [50, 10^{-7}, 1.4, 2.2]^T$ is shown in Fig. 6b. We can observe that by tuning the weight, fairness across the users can be greatly improved, though the sum-MSE is slightly compromised.

D. Robust vs Non-Robust Design

In this section, we assume $N_{\mathrm{U}}^i = 1, \forall\ i$ for the ease of illustration, and present the benefit of robust design under CSI uncertainty in LS-I. We plot the minimum SINR value as a function of the assumed user location, according to which we obtain $\{\hat{\boldsymbol{h}}_{i_kj}\}$. For a fixed assumed user location, 10^5 realizations of actual channel vectors are generated according to the error model Eq. (20) given a fixed ϵ or σ_e. The minimum

This article has been accepted for publication in a future issue of this journal, but has not been fully edited. Content may change prior to final publication. Citation information: DOI 10.1109/TCOMM.2018.2817222, IEEE Transactions on Communications

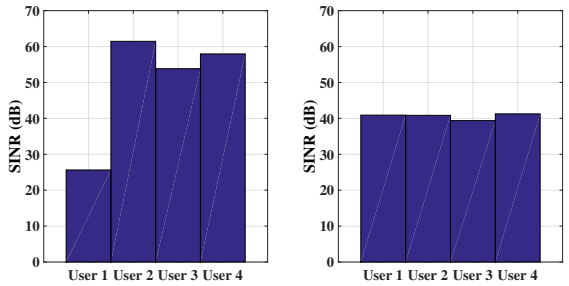

Fig. 6. (a) Left : $\boldsymbol{w} = [1, 1, 1, 1]^T$. (b) Right: $\boldsymbol{w} = [50, 10^{-7}, 1.4, 2.2]^T$.

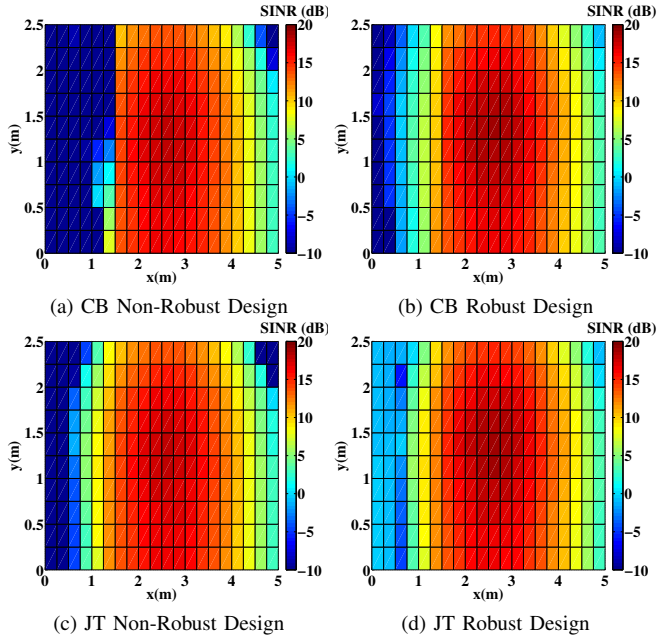

(a) CB Non-Robust Design (b) CB Robust Design

(c) JT Non-Robust Design (d) JT Robust Design

Fig. 7. Comparison between robust and non-robust design with the deterministic model for both JT and CB. $\epsilon = 10^{-5}$.

SINR value among those realizations can then be obtained. For concreteness, we further assume that the two users are symmetrically located on the plane of $z = 0.8$ m, i.e., the user coordinates are $(\pm x,\ y,\ 0.8)$ m for some x and y. Due to the symmetry, we only plot the SINR performance for one quadrant of the room in Fig. 7 and Fig. 8. From Fig. 7 and Fig. 8, we can observe that the robust design can improve the performance of CB compared with the non-robust approach, especially in the region where attocell boundaries lie. The robust approach improves the VLC transmitter design to avoid the large beamformer mismatch with the actual channels in spite of the CSI uncertainty, and keeps the SINR consistently high over the indoor environment, including attocell boundaries. We also include the performance of JT with and without robust design for benchmark purposes. Similar to CB, JT also experiences performance degradation resulting from CSI uncertainty. The SINR of the JT design is in general higher than its counterpart in CB especially for users at the attocell boundaries, which aligns with the results in Section VI-B.

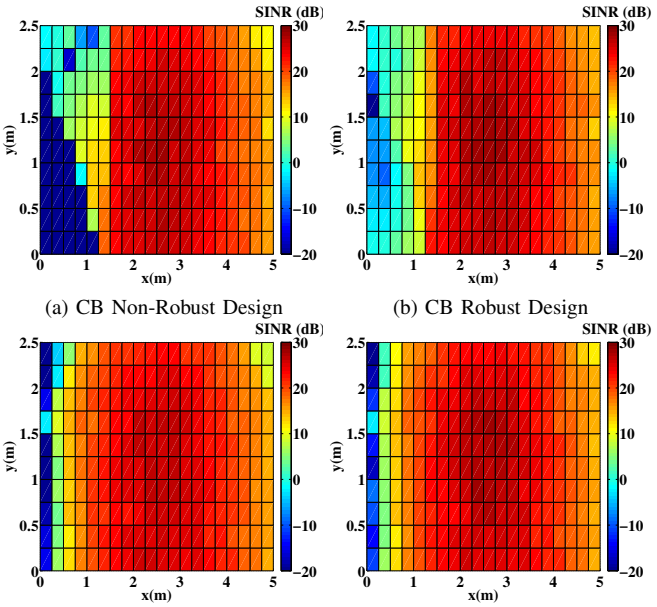

(a) CB Non-Robust Design (b) CB Robust Design

(c) JT Non-Robust Design (d) JT Robust Design

Fig. 8. Comparison between robust and non-robust design with the stochastic model for both JT and CB. $\sigma_e = 10^{-6}$.

VII. Conclusion

Attocell-edge users suffer from serious inter-attocell interference if universal frequency reuse is applied in VLC systems. Although joint transmission can be applied as a solution to this problem, it puts high requirements on the VLC infrastructure in terms of backbone capacity and inter-attocell synchronization. In this paper, an alternative solution, coordinated beamforming, has been proposed for interference mitigation in VLC downlinks, which requires less collaboration among attocells as compared to joint transmission. We focused on the beamforming design subject to the limited dynamic range of LED transmitters. Robust beamforming designs have also been investigated to combat the uncertainty in CSI. Numerical results validate the capability of the robust design against channel uncertainty and provide a preliminary evaluation around the potential practicality of coordinated beamforming in VLC systems. It shows that coordinated beamforming becomes a more preferable alternative to joint transmission as the number of luminaires per attocell increases, although the performance can degrade drastically with certain user distributions. A possible solution is to integrate coordinated beamforming with coordinated user scheduling, so that the wireless service providers can benefit from the architectural simplicity of coordinated beamforming while ensuring a comparable system performance to joint transmission. Further investigation regarding the integration is needed.

References

[1] H. Burchardt, N. Serafimovski, D. Tsonev, S. Videv, and H. Haas, "VLC: Beyond point-to-point communication," *IEEE Commun. Mag.*, vol. 52, no. 7, pp. 98–105, 2014.

[2] D. Tsonev, S. Videv, and H. Haas, "Light fidelity (Li-Fi): towards all-optical networking," in *SPIE OPTO*. International Society for Optics and Photonics, 2013, pp. 900 702–900 702.

[3] H. Haas, "High-speed wireless networking using visible light," *SPIE Newsroom*, vol. 19, 2013.

[4] C.-X. Wang, F. Haider, X. Gao, X.-H. You, Y. Yang, D. Yuan, H. Aggoune, H. Haas, S. Fletcher, and E. Hepsaydir, "Cellular architecture and key technologies for 5G wireless communication networks," *IEEE Commun. Mag.*, vol. 52, no. 2, pp. 122–130, 2014.

[5] H. Haas, L. Yin, Y. Wang, and C. Chen, "What is LiFi?" *J. Lightw. Technol.*, vol. 34, no. 6, pp. 1533–1544, 2016.

[6] H. Ma, L. Lampe, and S. Hranilovic, "Coordinated broadcasting for multiuser indoor visible light communication systems," *IEEE Trans. Commun.*, vol. 63, no. 9, pp. 3313–3324, 2015.

[7] M. B. Rahaim, A. M. Vegni, and T. D. Little, "A hybrid radio frequency and broadcast visible light communication system," in *IEEE GLOBECOM Workshops (GC Wkshps)*. IEEE, 2011, pp. 792–796.

[8] F. Jin, R. Zhang, and L. Hanzo, "Resource allocation under delay-guarantee constraints for heterogeneous visible-light and RF femtocell," *IEEE Trans. Wireless Commun.*, vol. 14, no. 2, pp. 1020–1034, 2015.

[9] X. Li, R. Zhang, and L. Hanzo, "Cooperative load balancing in hybrid visible light communications and WiFi," *IEEE Trans. Commun.*, vol. 63, no. 4, pp. 1319–1329, 2015.

[10] Y. Wang, D. A. Basnayaka, X. Wu, and H. Haas, "Optimization of load balancing in hybrid LiFi/RF networks," *IEEE Trans. Commun.*, vol. 65, no. 4, pp. 1708–1720, 2017.

[11] Z. Yu, R. J. Baxley, and G. T. Zhou, "Multi-user MISO broadcasting for indoor visible light communication," in *IEEE International Conference on Acoustics, Speech and Signal Processing (ICASSP)*, May 2013.

[12] T. Pham, H. Le Minh, and A. Pham, "Multi-user visible light communication broadcast channels with zero-forcing precoding," *IEEE Trans. Commun.*, 2017.

[13] Y. Hong, J. Chen, Z. Wang, and C. Yu, "Performance of a precoding MIMO system for decentralized multiuser indoor visible light communications," *IEEE Photon. J.*, vol. 5, no. 4, pp. 7 800 211–7 800 211, 2013.

[14] H. Ma, L. Lampe, and S. Hranilovic, "Robust MMSE linear precoding for visible light communication broadcasting systems," in *IEEE Global Communications Conference (Globecom)*, Atlanta, GA, USA, Dec. 2013.

[15] K. Ying, H. Qian, R. J. Baxley, and S. Yao, "Joint optimization of precoder and equalizer in MIMO VLC systems," *IEEE J. Sel. Areas Commun.*, vol. 33, no. 9, pp. 1949–1958, 2015.

[16] B. Li, J. Wang, R. Zhang, H. Shen, C. Zhao, and L. Hanzo, "Multiuser MISO transceiver design for indoor downlink visible light communication under per-LED optical power constraints," *IEEE Photon. J.*, vol. 7, no. 4, pp. 1–15, 2015.

[17] C. Chen, D. Tsonev, and H. Haas, "Joint transmission in indoor visible light communication downlink cellular networks," in *IEEE Globecom Workshops (GC Wkshps)*, 2013, pp. 1127–1132.

[18] D. Bykhovsky and S. Arnon, "Multiple access resource allocation in visible light communication systems," *J. Lightw. Technol.*, vol. 32, no. 8, pp. 1594–1600, 2014.

[19] B. Ghimire and H. Haas, "Self-organising interference coordination in optical wireless networks," *EURASIP Journal on Wireless Communications and Networking*, vol. 2012, no. 1, pp. 1–15, 2012.

[20] H.-S. Kim, D.-R. Kim, S.-H. Yang, Y.-H. Son, and S.-K. Han, "Mitigation of inter-cell interference utilizing carrier allocation in visible light communication system," *IEEE Commun. Lett.*, vol. 16, no. 4, pp. 526–529, 2012.

[21] S.-Y. Jung, D.-H. Kwon, S.-H. Yang, and S.-K. Han, "Reduction of inter-cell interference in asynchronous multi-cellular VLC by using OFDMA-based cell partitioning," in *18th IEEE International Conference on Transparent Optical Networks (ICTON),*, 2016, pp. 1–4.

[22] R. Bai, H. Tian, B. Fan, and S. Liang, "Coordinated transmission based interference mitigation in VLC network," in *IEEE 82nd Vehicular Technology Conference (VTC Fall), 2015*, 2015, pp. 1–5.

[23] M. Kashef, M. Abdallah, K. Qaraqe, H. Haas, and M. Uysal, "Coordinated interference management for visible light communication systems," *IEEE J. Opt. Commun. Netw.*, vol. 7, no. 11, pp. 1098–1108, 2015.

[24] K. Zhou, C. Gong, Q. Gao, and Z. Xu, "Inter-cell interference coordination for multi-color visible light communication networks," in *IEEE Global Conference on Signal and Information Processing (GlobalSIP)*, Dec 2016, pp. 6–10.

[25] X. Zhang, Q. Gao, C. Gong, and Z. Xu, "User grouping and power allocation for NOMA visible light communication multi-cell networks," *IEEE Commun. Lett.*, 2016.

[26] A. Tajer, N. Prasad, and X. Wang, "Robust linear precoder design for multi-cell downlink transmission," *IEEE Trans. Signal Process.*, vol. 59, no. 1, pp. 235–251, 2011.

[27] L. Venturino, N. Prasad, and X. Wang, "Coordinated linear beamforming in downlink multi-cell wireless networks," *IEEE Trans. Wireless Commun.*, vol. 9, no. 4, pp. 1451–1461, 2010.

[28] W. Yu, T. Kwon, and C. Shin, "Multicell coordination via joint scheduling, beamforming, and power spectrum adaptation," *IEEE Trans. Wireless Commun.*, vol. 12, no. 7, pp. 1–14, 2013.

[29] R. Zakhour and D. Gesbert, "Distributed multicell-MISO precoding using the layered virtual SINR framework," *IEEE Trans. Wireless Commun.*, vol. 9, no. 8, pp. 2444–2448, 2010.

[30] H. Elgala, R. Mesleh, and H. Haas, "Indoor optical wireless communication: potential and state-of-the-art," *IEEE Commun. Mag.*, vol. 49, no. 9, 2011.

[31] J. Grubor, S. C. J. Lee, K.-D. Langer, T. Koonen, and J. W. Walewski, "Wireless high-speed data transmission with phosphorescent white-light leds," *Proc. ECOC*, 2007.

[32] F. R. Gfeller and U. Bapst, "Wireless in-house data communication via diffuse infrared radiation," *Proceedings of the IEEE*, vol. 67, no. 11, pp. 1474–1486, 1979.

[33] T. Komine and M. Nakagawa, "Fundamental analysis for visible-light communication system using LED lights," *IEEE Trans. Consum. Electron.*, vol. 50, no. 1, pp. 100–107, 2004.

[34] H. Sampath, P. Stoica, and A. Paulraj, "Generalized linear precoder and decoder design for MIMO channels using the weighted MMSE criterion," *IEEE Trans. Commun.*

[35] C. B. Peel, B. M. Hochwald, and A. L. Swindlehurst, "A vector-perturbation technique for near-capacity multiantenna multiuser communication-Part I: channel inversion and regularization," vol. 53, no. 1, pp. 195–202, 2005.

[36] E. Bjornson, M. Bengtsson, and B. Ottersten, "Optimal multiuser transmit beamforming: A difficult problem with a simple solution structure [lecture notes]," *IEEE Signal Process. Mag.*, vol. 31, no. 4, pp. 142–148, 2014.

[37] C. Wengerter, J. Ohlhorst, V. Elbwart, and A. G. Edler, "Fairness and throughput analysis for generalized proportional fair frequency scheduling in OFDMA," in *IEEE 61st Vehicular Technology Conference*, vol. 3, 2005, pp. 1903–1907.

[38] J. Gorski, F. Pfeuffer, and K. Klamroth, "Biconvex sets and optimization with biconvex functions: a survey and extensions," *Mathematical Methods of Operations Research*, vol. 66, no. 3, pp. 373–407, 2007.

[39] "MOSEK," http://docs.mosek.com/8.0/toolbox/, accessed: 2017-03-30.

[40] J. Wang and D. P. Palomar, "Worst-case robust MIMO transmission with imperfect channel knowledge," *IEEE Trans. Signal Process.*, vol. 57, no. 8, pp. 3086–3100, 2009.

[41] M. B. Shenouda and T. N. Davidson, "On the design of linear transceivers for multiuser systems with channel uncertainty," *IEEE J. Sel. Areas Commun.*, vol. 26, no. 6, 2008.

[42] R. A. Horn and C. R. Johnson, "Matrix analysis," 1985.

[43] Y. C. Eldar, A. Ben-Tal, and A. Nemirovski, "Robust mean-squared error estimation in the presence of model uncertainties," *IEEE Trans. Signal Process.*, vol. 53, no. 1, pp. 168–181, 2005.

[44] European Norm (EN), "12464-1 (2011)," *Light and lighting. Lighting of work places. Part 1*.

[45] Luxeon, http://www.luxeonstar.com/lxw8-pw40-ansi-white-3985k-luxeon-rebel-led-190lm, [Online; accessed 27-June-2017].